Title: Morphology, Microstructure and Soft Magnetic Properties of Electrodeposited Fe-Ni-based Ternary Alloy Films

Brij Mohan Mundotiya[1]

1) Department of Metallurgical and Materials Engineering, Malaviya National Institute of Technology Jaipur, Jaipur, Rajasthan-302017, India.

Abstract

Soft magnetic films are used in many magnetic devices. They possess low coercivity and high magnetic permeability. Fe-Ni alloys are traditional soft magnetic materials widely used for the last few decades. However, these films have poor magnetic saturation and mechanical properties. These properties can improve by slightly including other transition metals such as Co, Cr, Mo, and W in the Fe-Ni-based alloy films. The electrodeposition technique is commonly employed for depositing Fe-Ni-based ternary alloy films. The properties of these ternary alloy films can be tuned by adjusting the deposition parameters such as current density, pH, temperature and concentration of electrolyte, and additives. This chapter provides a detailed overview of the various ternary alloy films based on Fe-Ni alloy and the influence of the deposition parameters on the magnetic properties.

Keywords: Coercivity, deposition parameters, soft magnetic materials, ternary alloys.

1. Introduction

The need for soft magnetic materials as a film over the bulk alloy system is driven by their numerous technical applications, such as micro-actuators, sensors, micromotors, and frictionless microgears. Soft magnetic materials are of interest because of low coercivity (H_C), high permeability, and magnetization. These properties are changed by changing the structure, internal strain, grain size (D), roughness, alloy composition, etc. The papers [1] by Herzer demonstrate the behavior between D and H_C. A relationship between H_C and D for different soft magnetic materials is shown in Figure *1*. The H_C of the magnetic materials rises by reducing the D and reaches a peak. Further decreasing in the D, the H_C again starts to fall. The behavior of the H_C with D is described as a domain configuration. The reduction in the D subdivides the materials into single-domain particles that increase the H_C towards a maximum. Although, the H_C decreases again for very small D, much smaller than the single domain size.

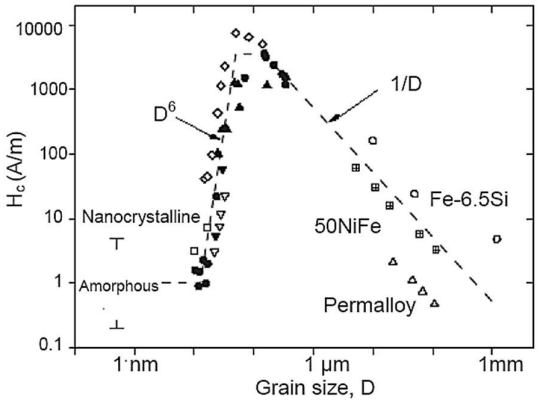

Figure 1 H_C vs. D for soft magnetic materials [2].

Fe-Ni-based alloys are typically utilized for high-frequency devices, including planar inductors, thin-film transformers, high-density recording media, and other devices. The key criteria for choosing materials for high-frequency devices are that they have high initial permeability, high saturation magnetization, high electrical resistivity, high magnetic remanence ratio, and low coercivity [3]. Potential choices are the Fe-Ni-based alloys because they have good electrical and soft magnetic properties [5]. The properties of Fe-Ni alloys might be improved even further by the slight inclusion of other transition metals. The addition of Co, Cr, Mo, and W in the Fe-Ni-based ternary alloy has attracted significant attention.

The Fe-Ni-based alloy may be deposited using several techniques, including electroless deposition, electrodeposition, sputtering, molecular beam epitaxy, and evaporation. The electrodeposition approach is the most popular of these well-known techniques because of its low equipment cost, high deposition rate, and control over the film's thickness and grain size. The focus on the electrodeposition of the Fe-Ni-based alloy is due to its cost-effective and simple method, as well as the Fe-Ni-based alloys, which have stable and unique magnetic properties. In addition, they should have outstanding tribological behaviors for electronic applications. However, the Fe-Ni alloy films have poor mechanical properties [6]. Adding Co, Cr, Mo, and W could improve the mechanical and magnetic properties. The magnetic characteristics of Fe-Ni-based films electrodeposited with Co, Cr, W, and Mo are discussed in this chapter.

2. Electrodeposition Process

The electrodeposition of film on the substrate works on the principle of Faraday's law of electrolysis. An electrochemical cell is necessary to deposit thin films using the electrodeposition method. Electrodes (cathode and anode), electrolyte, interconnects, and a power supply are its constituent parts. Figure 2 illustrates a schematic of the electrochemical cell. The cathode and anode are the negative and positive terminals in the electrochemical cell, respectively. When the external power source connects, a current flows from the anode to the cathode. Positive metal ions travel in the direction of the cathode surface during the current flow. A continuous reduction of metal ions on the cathode surface takes place and forms uniform or island-type films that depend on the nucleation and growth mechanism. The following chemical reactions occur at the anode and cathode in the electrochemical cell.

$$Cathode: \quad M^{n+} + ne^- \rightarrow M$$

$$Anode: \quad M \rightarrow M^{n+} + ne^-$$

Where M, M^{n+}, and n are the metal, metal ions, and number of electrons transferred in the cell reactions, respectively. In the electrochemical cell, the anode can be categorized into two types: (a) consumable anode and (b) permanent anode. The consumable anode sacrifices by giving the metal ions to the electrolyte that maintains ions concentration in the electrolyte. However, the permanent anode is only used to complete the circuit of the electrochemical cell.

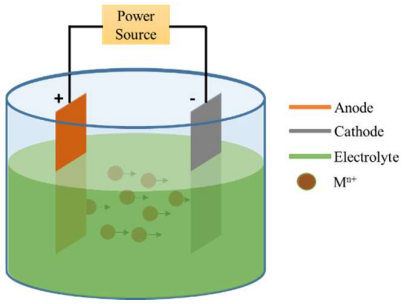

Figure 2 Schematic diagram of an electrochemical cell.

2.1 Electrolytic solution for the Fe-Ni-based alloy films

The Fe-Ni-based alloy films have been deposited using a variety of electrolytic solutions, including chloride [6], sulfate [13], fluorborate [14], and sulphamate [16]. All these electrolytes consist of the Fe in the Fe(II) states, and the presence of the Fe(III) state is undesirable. Fe(III)-states in the electrolyte reduce the cathode efficiency for metal deposition and may produce brittle, strained, and pitted deposited films [18]. In the industry and for scientific research, sulfate- and chloride-based electrolytes are extensively employed. These electrolytes are also economical for the deposition of Fe-Ni-based alloy films. In sulfate electrolytes, Ni chloride is commonly added to increase the conductivity of the electrolyte. However, the absence of chloride in the sulfate electrolyte results in low internal stresses in the deposited films. Besides the sulfate electrolyte, chloride electrolytes are also employed to deposit the Fe-Ni-based alloy films. The films deposited from the chloride electrolyte are harder and have more stress than those deposited from the sulfate electrolyte [19]. These electrolytic solutions also have significant drawbacks. When the deposition temperature exceeds 85 °C, hydrochloric acid will massively evaporate from the chloride electrolyte. Conversely, forming a Fe-Ni alloy film from the sulfate electrolyte at a high deposition rate is challenging.

Additives, such as citrate, thiourea, and saccharine, are introduced into the electrolyte to influence the deposition morphologies, structure, and/or deposition quality. Citrate additions in an electrolyte might alter the properties of the deposited layer since they contain active carbon. Also, the rate of dissolution of the consumable Ni or Ni-metal electrode cannot be compensated by the reduction of the Ni ions in the citrate-containing electrolyte. A fluorborate electrolyte can be used to overcome these difficulties since Ni ions dissolve quickly in it, compensating for the reduction of Ni ions in the electrolyte. Nevertheless, fluorborate electrolyte has drawbacks due to its high cost and corrosiveness. A fluoride wastewater

treatment plant is required before the disposal of electrolytes [6]. On the other hand, sulphamate electrolytes have some notable benefits, such as strong throwing power and a high deposition rate. The deposited films have low internal stresses. This electrolyte does have certain drawbacks, though. It generates azodisulfonate, the primary sulfur source, which reduces ductility and compressive stresses. [19].

The concentration of the electrolytes that are often used to deposit Fe-Ni alloy films

Type of electrolyte	Electrolyte bath	pH	Temperature (°C)	Current density (mA/cm^2)	Substrate	Reference
Chloride based	$FeCl_2 \cdot 4H_2O$: 2.25 M $FeCl_3 \cdot 6H_2O$: 0.75 M H_3BO_3: 0.25 M HCl: 4 ml/l $NiCl_2 \cdot 6H_2O$: 0.1-1.0M	-	80	100 – 800	Pure Ti circle plate	Su et al. [6]
Chloride based	$FeCl_2 \cdot 6H_2O$: 1-2.1 g/l H_3BO_3: 25 g/l $NiCl_2 \cdot 6H_2O$: 23.5 g/l	2.5	55.5	20	Steel 4130	Abdel-Karim et al. [20]
Sulfate based	$FeSO_4 \cdot 7H_2O$: 150 g/l $NiSO_4 \cdot 7H_2O$: 15 g/l NaCl: 10 g/l H_3BO_3: 45 g/l Saccharin: 2.5 g/l Additives: 1.5 g/l	3.3	57	30	Cu sputtered Si wafer	Wei et al. [4]
Sulfamate-Chloride based	$Ni(H_2NSO_3)_2 \cdot 4H_2O$: 0.2 M $FeCl_2 \cdot 4H_2O$: 0.01 – 0.04 M H_3BO_3: 0.4 M Sodium Saccharin: 1.5 g/l Sodium dodecyl sulfate: 0.2 g/l Ascorbic acid: 1.0 g/l	3.0	23	20 – 100	Platinum	Leith et al. [21]

The concentration of the electrolytes that are often used to deposit Fe-Ni-Cr alloy films

Type of electrolyte	Electrolyte bath	pH	Temperature (°C)	Current density (mA/cm^2)	Substrate	Reference
Chloride based	$CrCl_3 \cdot 6H_2O$: 200 g/l $NiCl_2 \cdot 6H_2O$: 50 g/l $FeCl_2 \cdot 4H_2O$: 40 g/l $Na_3C_6H_5O_7$: 70 g/l $AlCl_3$: 130 g/l	0.3	30	50 – 150	Copper plate (70 mm x 25 mm x 1 mm)	Adelkhani et al. [9]
Chloride based	$CrCl_3 \cdot 6H_2O$: 0.80 mol/dm^{-3} $NiCl_2 \cdot 6H_2O$: 0.20 mol/dm^{-3}	1.8	20	-	Copper (25 mm x 25 mm x 0.2 mm)	Sziraki et al. [22]

	$FeCl_2 \cdot 4H_2O$: 0.02 mol/dm^{-3} NaCl: 0.50 mol/dm^{-3} NH_4Cl: 0.50 mol/dm^{-3} H_3BO_3: 0.15 mol/dm^{-3} 500 g H2O deionized and 500 g DMF					
Chloride based	$CrCl_3 \cdot 6H_2O$: 0.4 mol/l $NiCl_2 \cdot 6H_2O$: 0.2 mol/l $FeCl_2 \cdot 4H_2O$: 0.03 mol/l Glycine: 0.4 mol/l NH_4Cl: 0.5 mol/l H_3BO_3: 0.15 mol/l NaCl: 0.5 mol/l	1.0	22	-50 – -100	Cr (5 nm)/Au (100 nm) sputtered Si-substrate	Bertero et al. [23]
Sulfate - Chloride based	$CrCl_3 \cdot 6H_2O$: 213 g/l $NiCl_2 \cdot 6H_2O$: 47.54 g/l $FeSO_4 \cdot 7H_2O$: 11.15 g/l Sodium citrate: 58.8 g/l Glycine: 60 g/l Formic acid: 14.1 g/l	-	30	15 – 25	Cu cylinder	Huang et al. [24]
Chloride based	$NiCl_2 \cdot 6H_2O$: 0.04 – 0.16 mol/l $CrCl_2 \cdot 6H_2O$: 0.37 – 0.5 mol/l $FeCl_2 \cdot 4H_2O$: 0.025 – 0.05 mol/l NH_4Cl: 0.90 mol/l H_3BO_3: 0.48 mol/l KBr: 0.14 mol/l $Na_3C_6H_5O_7 \cdot 2H_2O$: 0.25 mol/l HCOOH: 0.75 mol/l $C_2H_4O_3$: 0.65 mol/l	1	30	10 – 40	Copper	Tavoosi and Barahimi [25]

The concentration of the electrolytes that are often used to deposit Fe-Ni-Co alloy films

Type of electrolyte	Electrolyte bath	pH	Temperature (°C)	Current density (mA/cm^2)	Substrate	Reference
Sulfate based	$CoSO_4 \cdot 7H_2O$: 0.075 mol/l $NiSO_4 \cdot 7H_2O$: 0.2 mol/l $FeSO_4 \cdot 7H_2O$: 0.03 mol /l H_3BO_3: 0.4 mol /l	1.5-3.0	Room temperature	3 – 40	Cu(250 nm)/Cr(25 nm)/ SiO_2(300 nm)/Si substrate	Khomenko et al. [26]
Chloride based	$FeCl_2 \cdot 6H_2O$: 1.275 mol/l $CoCl_2 \cdot 6H_2O$: 0.225 mol/l	0.34 – 5	23 – 90	5	Cu sheet	Park et al. [27]

	$NiCl_2 \cdot 6H_2O$: 0.02 mol/l $CaCl_2$: 1.0 mol/l L-Ascorbic acid: 0 or 0.05 mol/l					
Sulfate based	$FeSO_4 \cdot 7H_2O$: 15 g/l $NiSO_4 \cdot 7H_2O$: 260 g/l $CoSO_4 \cdot 7H_2O$: 20 g/l NaCl: 8 g/l H_3BO_3: 30 g/l Saccharin: 1.5 g/l Additives: 1.2 g/l	3.5	60	10	Cu sputtered Si wafer	Wei et al. [4]
Sulfate based	$FeSO_4$: 0.025 mol/l $CoSO_4$: 0.05 mol/l $NiSO_4$: 0.2 mol/l	2.5	Room temperature	-	GaAs (100) substrate	Sun et al. [28]

The concentration of the electrolytes that are often used to deposit Fe-Ni-W alloy films

Type of electrolyte	Electrolyte bath	pH	Temperature (°C)	Current density (mA/cm^2)	Substrate	Reference
Alkaline sodium citrate based	$NiSO_4 \cdot 7H_2O$: 0.06 mol/l $FeSO_4 \cdot 7H_2O$: 0.02 mol/l $Na_2WO_4.2H_2O$: 0.15 mol/l $Na_3C_6H_5O_7.2H_2O$: 0.30 mol/l NH_4Cl: 0.50 mol/l Boric acid: 1.0 mol/l Saccharin sodium: 0.08 mol/l NaBr: 0.15 mol/l Sodium Laurel Sulfate: 0.087 mol/l	8.0	65	40	Copper foils and low carbon low alloy steels sheets	Sriraman et al. [29]
Sulfate based	Iron sulfate: 0.0115-0.10 mol/l Nickel sulfate: 0.012-0.20 mol/l Sodium tungstate: 0.03-0.12 mol/l Citric acid: 0.028-0.19 mol/l Boric acid: 0.16 mol/l YC-4: 3-10 ml/l	8	80	40-100	AISI A3 steel and AISI 1045 steel	He et al. [30]
Sulfate based	Nickel sulfate: 0.15 mol/l, Ferrous sulfate: 0.005 mol/l Sodium tungstate: 0.6 m·mol/l Diammonium H-citrate: 0.16 mol/l	8	Room temperature	5	Cr-NiFe sputtered Si wafer	Mundotiya et al. [31]

	Citric acid: 0.08 mol/l Boric acid: 0.12 mol/l Saccharin: 0.05 mol/l					
Ammonium citrate based	$NiSO_4 \cdot 7H_2O$: 0.012 mol/dm^3 $FeSO_4 \cdot 7H_2O$: 0.004 mol/dm^3 $Na_2WO_4 \cdot 2H_2O$: 0.01 mol/dm^3 $Na_3C_6H_5O_7 \cdot 2H_2O$: 0.06 mol/dm^3 NH_4Cl: 0.5 mol/dm^3 H_3BO_3: 1.0 mol/dm^3 NaBr: 0.15 mol/dm^3	11.7 – 12	50 – 70	500 – 1000	Titanium	Zelenovic et al. [32]

The concentration of the electrolytes that are often used to deposit Fe-Ni-Mo alloy films

Type of electrolyte	Electrolyte bath	pH	Temperature (°C)	Current density (mA/cm^2)	Substrate	Reference
Sulfate based	$NiSO_4 \cdot 6H_2O$: 100 g/l $FeSO_4 \cdot 6H_2O$: 5 g/l NaCl: 35 g/l H_3BO_3: 40 g/l $Na_3C_6H_5O_7 \cdot 2H_2O$: 70 g/l $Na_2MoO_4 \cdot 2H_2O$: 20 g/l	4.0	30	600	Nickel foam (10 mm x 10 mm x 0.5 mm)	Huang et al. [33]
Citrate based	Nickel sulfate: 60 g/l Ferrous sulfate: 30 g/l Sodium molybadate: 10 g/l Diammonium citrate: 60 g/l Citric acid: 5.5 g/l Boric acid: 10 g/l	8	60, 70, 80	0.01	Mild steel	Kannan et al. [34]
Citrate based	$NiSO_4 \cdot 6H_2O$: 60 g/l $FeSO_4 \cdot 7H_2O$: 4 g/l $Na_2MoO_4 \cdot 2H_2O$: 2 g/l NaCl: 10 g/l Citric acid: 66 g/l Saccharine: 3 g/l	1.5	Room temperature	30	Au/Cr sputtered glass	Zhou et al. [35]
Chloride based	$NiCl_2 \cdot 6H_2O$: 100 mM $Na_2MoO_4 \cdot 2H_2O$: 20 mM $C_5H_5Na_3O_7 \cdot 2H_2O$: 300 mM $FeCl_2 \cdot 4H_2O$: 0 – 18 mM	6	Room temperature	40-80	Cu	Badrnezhad et al. [36]
Sulfate based	$NiSO_4 \cdot 6H_2O$: 64 g/l $FeSO_4 \cdot 7H_2O$: 16 g/l	9.8	30	5-60	Copper or Nickel	Hu et al. [37]

	$Na_2MoO_4 \cdot 2H_2O$: 9.6 g/l Citric acid: 52.8 g/l					

3. Electrodeposition parameters and magnetic properties of Fe-Ni-based alloy films

3.1 Fe-Ni alloy films

The magnetic properties of Fe-Ni alloys having 40 to 90 wt.% Ni are very interesting, mainly when the alloy includes 78.5 wt.% Ni. Permalloy, a Fe-78.5Ni alloy, has exceptionally high magnetic permeability, low magnetic anisotropy values, and magnetostriction parameters under weak magnetic fields. The heat treatment procedure can somewhat modify these alloys' magnetic properties. The alloy undergoes structural, internal, and other changes throughout the heat treatment process.

The potential phases and phase transformations are correlated in Figure 3. The reduction in temperature demonstrates the existence of two successive phase transformations. The two subsequent phase transformations are (a) the second kind of paramagnetic-ferromagnetic transition (at the Kurnakov points) and (b) the first kind of order-disorder transformation (at the Curie points) under the symmetries of $L1_2$-type or $L1_0$-type ordered and A1-type disordered phases. The $L1_2$-type structure is observed in Ni_3Fe stoichiometry, while the $L1_0$-type structure is observed in the equiatomic NiFe stoichiometry. The A1-type structure originated in a FCC solid solution of Fe and Ni [38]. The magnetic transition and structural phase-transformation points, also known as the Curie and Kurnakov points, are affected by the amount of Fe in the solution. The Curie and Kurnakov points decline with an increase of the Fe content. Fe-Ni system contains very little information at low temperatures because the diffusion of Ni in Fe-Ni is slow [39].

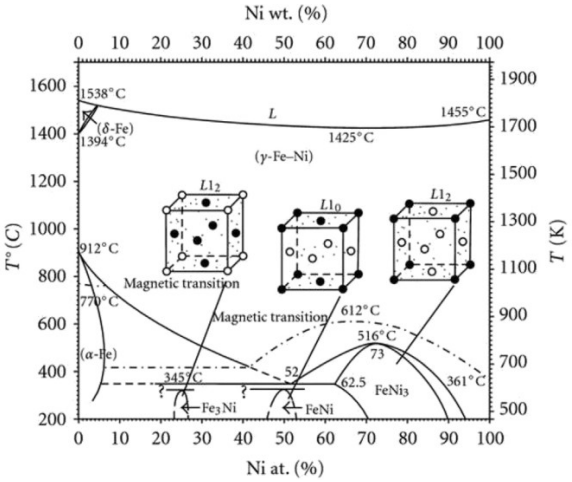

Figure 3 Fe-Ni binary phase diagram [38].

The anomalous co-deposition phenomena causes the Fe-Ni alloy to deposit on the substrate. Brenner introduces the concept of anomalous co-deposition. According to this concept, Fe is deposited more frequently than Ni, a more noble metal. In the unusual event, the reduction process forms nickel hydroxide and catalystic iron hydroxide. With increasing Fe^{2+} ions in the

electrolyte, the concentration of catalystic iron hydroxide increases and surpasses that of nickel hydroxide. The deposition mechanism of Fe-Ni alloy is given below [40]:

$$Fe^{2+} + OH^- \leftrightarrow FeOH^+ \; and \; Ni^{2+} + OH^- \leftrightarrow NiOH^+ \quad (1)$$

$$FeOH^+ + e^- \leftrightarrow FeOH_{ad} \; and \; NiOH^+ + e^- \leftrightarrow \; NiOH_{ad} \quad (2)$$

$$FeOH_{ad} + e^- \leftrightarrow Fe + OH^- and \; NiOH_{ad} + \; e^- \leftrightarrow Ni + OH^- \quad (3)$$

The above reactions indicate that adsorbed metallic hydroxide forms before reducing Fe and Ni ions. The content of $FeOH^+$ is significantly larger than $NiOH^+$ because of the significant inequality between the dissociation constant. Thus, the $FeOH_{ad}$ began to occupy the $NiOH_{ad}$ adsorption site. This has the effect of partially inhibiting Ni atom deposition.

Figure 4 depicts the XRD pattern of Fe-Ni alloy with varying Fe content. Fe-Ni alloys are dominated by FCC structure at lower Fe contents since Ni possesses an FCC structure. The pattern demonstrates that when the Fe content rises to 7.6 at.%, the intensity of the (220) peak increases while the intensity of the (111) peak falls. A BCC phase appears at 40.4 at.% Fe. The peak broadening at 44.7° suggests that the Fe-Ni alloy comprises a mixture of FCC(111) and BCC(110) phases. [41].

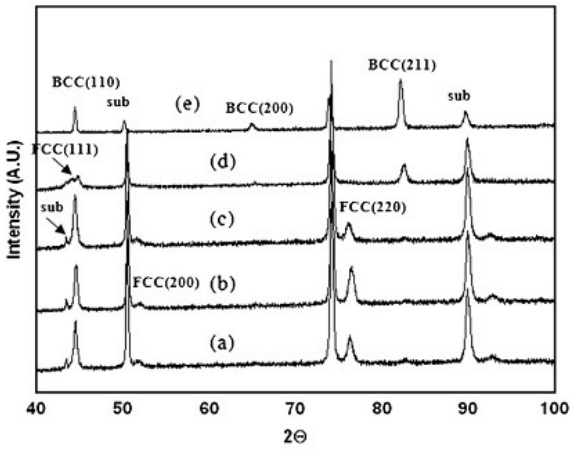

Figure 4 XRD pattern of the Fe-Ni alloy with various compositions at electrolyte temperature of 70°C: (a) 6.7Fe93.3Ni, (b) 7.6Fe92.4Ni, (c) 14.0Fe86.0Ni, (d) 40.4Fe59.6Ni, and (e) 95Fe5Ni [41].

The Fe content present in Fe-Ni alloy films significantly impacts the magnetic properties. The properties and composition of Ni-Fe alloy may be tuned by altering the deposition parameters (i.e., applied current density, electrolyte concentration and temperature, electrolyte pH, and additional agents). According to Su and Qiang's [42] research, more Ni content is deposited when the Ni ions in the electrolyte increase and the pH falls from 2.1 to 4.3. The saturation magnetization decreases as the Ni content rises in films. The H_C, on the other hand, declines with Ni concentration in the range of 0.38 to 0.55, approaches a minimum of 43.14 Oe at 0.55 at.% Ni, and subsequently increases with increasing Ni content. It could be explained by the fact that two factors might affect the coercivity: (a) the presence of imperfections and (b) the high Ni content in films. The H_C of Fe-Ni alloy films being deposited varies similarly to that

of the mean internal stresses, in the opposite direction of the crystallites size, and similarly to that of the grain boundaries density. The leading causes of high H_C are internal stresses and grain boundary density. The H_C rises due to the pining of the magnetic domain walls at the grain boundaries. Koo and Yoo [41] reported that the crystallite grain size and internal stresses depend on Fe content in the Fe-Ni alloy films (Figure 5). Figure *5* demonstrates that the Fe-Ni alloy film at ~ 40 at.% of Fe has maximum stress because the grain size is smallest at this composition.

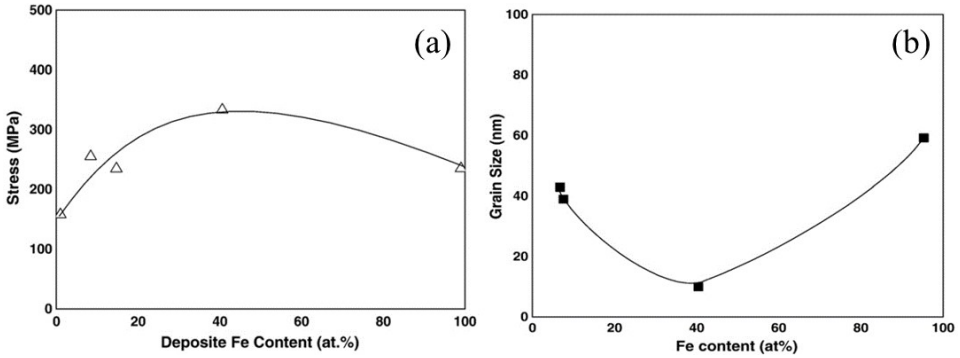

Figure 5 Variation of (a) stress and (b) grain size in Fe-Ni alloy films [41].

The Ni content in the films also influences by the organic additives used in the electrolyte. Shimokawa et al. [43] studied that By raising the citric acid concentration in the citric-based electrolyte from 0 to 100 g/l, the Fe content elevates from 18 to 50%. However, lifting the citric acid concentration from 0 to 30 g/l lowers H_C from 380 to 20 A/m. The addition of saccharin in the electrolyte causes a reduction in the size of the crystallites/grains and internal stresses in the deposited films. However, the composition of Fe-Ni alloy films is only marginally impacted by saccharin. Simultaneously, saccharin significantly affects the magnetic properties. The H_C, correlated with crystallite size and internal stresses, is reduced considerably by adding saccharin to the electrolyte. The H_C of films is low at low internal stresses [44]. Contrarily, saccharin raises the sulfur content in the deposited films, which is not dissolved in Fe-Ni alloys. When the coating has been subjected to high temperatures, the sulfur segregates on the grain boundaries, encouraging intergranular fracture and grain boundary embrittlement [45].

3.2 Fe-Ni-Cr alloy films

The Fe-Ni-Cr alloy films exhibit fascinating and distinctive properties for many applications. Fe-rich Fe-Ni-Cr alloy films exhibit good corrosion resistance, whereas Ni-rich alloy films exhibit unique magnetic properties. The high Cr content in these films will have the same high hardness and corrosion resistance as pure Cr [9]. Furthermore, these alloy films are an attractive choice for constructing low-cost bio-devices because of their resistance to harsh conditions and excellent biocompatibility. [46].

According to Huang et al. [24], Fe-rich Fe-Ni-Cr films are crystalline, whereas Cr-rich Fe-Ni-Cr films are amorphous. For the Cr-rich Fe-Ni-Cr alloy films deposited at 20 and 25 A/dm^2, the XRD diffraction pattern exhibits no diffraction pattern. A widened peak of (110) is seen for Fe-rich alloy films deposited at 15 A/dm^2, as illustrated in Figure 6. Tavoosi and Barahimi [25]

have also explored that the Fe-Ni-Cr alloy films deposited at current densities below 20 A/dm^2 consist of Fe-γ and amorphous phases. A crystalline solid solution of Fe-Ni-Cr is called Fe-γ. The Fe-γ phase peak has vanished beyond 30 A/dm^2, and an amorphous phase is present.

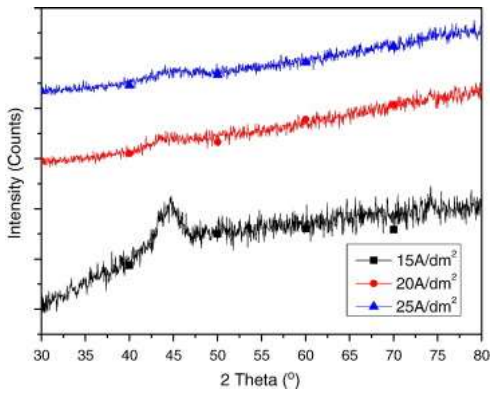

Figure 6 XRD pattern of the Fe-Ni-Cr alloy films [24].

The current density also influences the morphologies of these deposited films. Network fractures and the characteristic nodular morphology are visible at lower current densities in the deposited films. The size and number of these features increase with increasing the deposition current density (see Figure 7). The content of Cr in these alloys reduces the quality by forming cracks and generating high internal stresses. It can be difficult to prevent or minimize cracking in Fe-Ni-Cr alloy films, which reduces the maximum feasible coating thickness. The inclusion of CrH and/or CrH_2 in the deposited films, which later disintegrate into metallic Cr and hydrogen gas, causes shrinkage in it. This shrinkage contributes to the crack generation in the deposited films [47]. To overcome these problems, organic additives such as saccharin are introduced in the electrolyte to decrease internal stresses and improve deposit quality. But, the addition of the organic additives will reduce the corrosion resistance because they hinder the creation of a passive oxide layer on the surface [48].

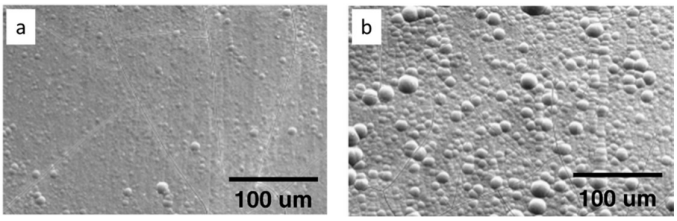

Figure 7 Morphology of Fe-Ni-Cr alloy films deposited at (a) 15 A/dm^2 and (b) 25 A/dm^2 [24].

The electrodeposited amorphous-like Fe-Ni-Cr films are ferromagnetic in contrast to the traditional Fe-Ni-Cr alloys, which exhibit a non-magnetic property. The H_C value between 5 and 40 Oe is seen in all deposited Fe-Ni-Cr alloy films, and saturation magnetization falls linearly with Cr content. The deposited films become non-magnetic when the Cr content exceeds 40 wt.% [23]. The decrease in the magnetic saturation is due to decreased Fe-Fe exchange interactions and enhanced interactions between Fe and Cr atoms. As a result of the antiferromagnetic interaction between Fe and Cr atoms, the magnetic saturation of the formed films is further reduced [49].

Adelkhani et al. [9] have investigated that current density influences the film composition. The content of the Fe and Ni is decreased by raising the current density from 5 to 15 A/dm^2, but Cr shows the opposite tendency. With increasing current density, the metal ions Ni^{2+} and Fe^{2+} reduction occurs predominantly under diffusion control and reaches a minimal value. Although, the reduction of the Cr^{3+} ions depends on the thermodynamic characteristics of the Cr. The thermodynamic properties indicate that the deposition of Cr takes place at a greater deposition overpotential than the Fe and Ni deposition. The deposition overpotential is directly proportional to the current density. As a result, raising the current density raises the Cr content. Similar behavior is also demonstrated by several researchers [7]. Moreover, the grain refinement process is positively impacted by the current density, which results in a reduction in grain size. The decrease in the grain size is due to an enhancement in the nucleation rate that overcomes the grain growth rates. As current density increases from 10 to 50 mA/cm^2, the grain size of Fe-Ni-Cr alloy films decreases from 64 to 38 nm. Fe-Ni-Cr alloy films exhibit higher Cr content and smaller grain size at high deposition current densities that result in low saturation magnetization and high H_C.

The H_C of Fe-Ni-Cr alloy films depends on several factors, such as grain size (D), microstructure, and chemical composition. Out of these factors, the D is the most influential parameter that influences the H_C. If D exceeds the magnetic exchange length, the domain wall pinning occurs along the grain boundaries, resulting in high coercivity in the deposited films. However, the H_C decreases when D is below the exchange length because the domain wall effect is crossed out, and each grain act as a single domain. The exchange length depends on the Fe content and reduces with a drop in the Fe. For Fe-Ni permalloy, the exchange length is 14 – 28 nm [51]. The H_C of the deposited films is increased from 157.6 to 356.0 A/m by increasing the current density from 64 to 38 nm [7]. It shows that the grain size of these films is above the exchange length. Fe has the best magnetic properties, and the amount of Fe in Fe-Ni-Cr ternary alloy coatings affects their magnetic behavior. Ni is another important element that has soft magnetic characteristics. As a result, saturation magnetization rapidly decreases as Fe and Ni content is reduced.

3.3 Fe-Ni-Co alloy films

Fe-Ni-Co alloy films have been widely explored as soft magnetic materials because they have better properties when compared to Fe-Ni alloy. Fabricating the Fe-Ni-Co alloy films with high saturation magnetization (>2 T) and low H_C by the electrodeposition process is challenging. Also, the deposition of ternary alloy by the electrochemical process is complex because the composition and magnetic properties depend on the deposition parameters, such as electrolyte pH and temperature, additives, deposition time, and electrolyte ionic concentrations. The composition and microstructure of the deposited films can be regulated by adding different additives. The additives include sulfur, thiourea, sodium lauryl sulfate, boron/phosphorous, saccharin, sodium dodecyl sulfate, Triton X-100, 1-dodecyl-3-methylimidazolium chloride. Mardani et al. [52] have reported the effect of three different surfactant additives on the deposited Fe-Ni-Co alloy film. The additions include Triton X-100, an anionic surfactant; sodium dodecyl sulfate (SDS), a nonionic surfactant; and 1-dodecyl-3-methylimidazolium chloride (IL), a cationic surfactant. The deposited films are compact, smooth, bright, and crack-

free, but different morphologies are obtained. Zhang and Ivey [53] have explored the ammonium citrate additive effect on properties. The Fe-Ni-Co alloy film has relatively high H_C deposited from an electrolyte with no ammonium citrate. On the other hand, low citrate concentrations cause the H_C to decrease; a citrate concentration of 30 g/L results in a minimum H_C of 18 Oe. It can be attributed that the citrate bath results in low stress in the deposited films. The ammonium citrate forms citrate-complex ions in the electrolyte, delaying metal atom deposition. Adatoms can fit into preferred lattice locations more frequently. As a result, they lead to a structure with fewer imperfections and less stress. However, the H_C rapidly rises when the citrate concentration exceeds 30 g/L.

The film thickness is another vital parameter on which coercivity depends. Tabakovic's group [54], have been reported an expression that relates to the film thickness (t) and H_C of Fe-Ni-Co alloy film:

$$H_C = Ct^{-n}$$

where C is a constant and n=4/3. For Fe-Co-Ni alloy films with thicknesses between 100 nm to 1000 nm, the value of n is around 1. [28]. The H_C declines with the rise in t. There may be minor departures from this trend due to structure and composition changes.

The B_S of these films is much higher than Fe-Ni alloy films. According to Khomenko et al. [26], the enhancement in the B_S may come from various causes. One might include rearranging the atomic orbitals to maintain the maximum possible magnetic moment by aligning the spins that are subjected to the exchange forces. Rearranging the structure in response to changes in the chemical composition can be another source. The change in the chemical composition causes competition between the BCC and FCC phases or structural modifications. According to Ohashi et al. [56], the Co65Ni12Fe23 films with mixed BCC and FCC phases had a higher B_S 2.0 – 2.1 T than Co65Ni12Fe23 films with BCC phases. Similar behavior was also observed in the Co52Fe26Ni22 alloy film that consists of the mixed BCC and FCC phases [57].

Bozorth [58] has reported a composition-B_S diagram of Fe-Ni-Co ternary alloy. Figure 8 shows that the maximum values of the B_S are obtained around Fe60Co40 composition; however, they do not procure low H_C. Thus, it is focused on depositing Fe-Ni-Co ternary alloy films with high B_S and low H_C. Osaka [59] has presented a compositional diagram, as shown in Figure 9, with regions of low $H_C < 2$ Oe. From Figure 8 and Figure 9, the low H_C values obtained in the Co-rich composition regions B and C are located nearly in the region where $B_S > 1.8$ T, while A region belongs to the low B_S region. The higher value of B_S in regions B and C is considered that these films have a minimal amount of sulfur.

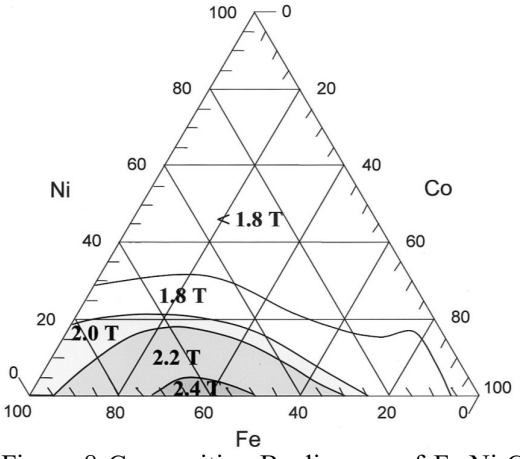

Figure 8 Composition-B_S diagram of Fe-Ni-Co ternary alloy [58].

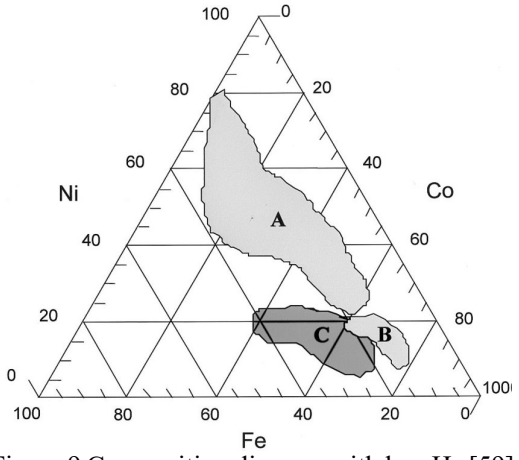

Figure 9 Composition diagram with low H_C [59].

The Fe ion concentrations have an impact on the Fe-Ni-Co film composition, according to Kockar et al. [60]. With an increase in the Fe ion concentrations, the Fe and Co rise while their Ni contents fall. The magnetic saturation is enhanced from 1.08 T to 1.36 T, and H_C is decreased from 60 Oe to 13 Oe with increasing Fe and Co contents and lowering Ni content in the films,.

Magnetic properties of Fe-Ni-Co alloy films are influenced by internal stress and play a vital role in incorporating these materials into magnetic devices. High magnetic stresses in the films may fail these devices due to the loosening/unconnection of film from the substrate. Saito et al. [61] have studied that the internal stress of Co-rich Fe-Ni-Co alloy films (60-70 at.% Co, 8-15 at.% Ni, and 15-27 at.% Fe) reduces from ~ 800 to ~ 500 MPa by enhancing the annealing temperatures up to 250 °C. Rasmussen et al. [62] have determined the stresses of the pulse-reverse electrodeposited Co-rich alloy films at a deposition temperature of 40 ℃ and pH of 3.9 – 4.2. The deposited FeNiCo film has stresses in the range of 69-101 MPa.

3.4 Fe-Ni-W alloy films

The addition of W improves the microhardness, wear resistance, and magnetic properties of Fe-Ni alloys. It has been investigated by He at el. [30] that the W concentration affects the morphologies of the deposited film. At 18 wt% of W, Fe-Ni-W alloy films are smoothed. The surface gets significantly rougher and microcracks appear above this W content. The high content of W introduces more internal stresses; thus, the Fe-Ni-W alloy films are more fragile. Zelenovic et al. [32] deposited the Ni-24%Fe-11%W powders by electrodeposition process. The current density and electrolyte temperature did not affect these powders' composition because the codeposition of the Ni, Fe, and W is controlled by the slow diffusion of their electroactive species. The effect of pH on the alloy film composition has been studied by Donten et al. [63]. The optimal pH range for the deposition of Fe-Ni-W alloy films is 5-10. A pH greater than 10 causes the creation of iron hydroxides, which lowers the Fe^{2+} ions in the electrolyte solution, whereas a pH lower than 5 causes the development of precipitated tungstic acid.

The impact of substrate temperature on the properties of Fe-Ni-W alloy films has been shown by Mundotiya et al. [31]. The alloy films deposited at a substrate temperature value of 5 ºC have low coercivity and high permeability of 257 A/m and 487, respectively, compared to those deposited at 10 ºC and 21 ºC. Furthermore, when the temperature rises, the internal stresses and roughness of the formed films also increase. The H_C increases with temperature because the internal stresses and surface roughness also act as a barrier to the movement of the magnetic domain wall. Citrate addition to the electrolyte affects the internal stresses of the deposited Fe-Ni-W alloy films [64]. By raising the citrate content, the coercivity of the deposited films increases. The increase in coercivity is due to changes in the stresses. The stress is compressive. Compressive stresses lead to high coercivity, while tensile stresses reduce coercivity.

3.5 Fe-Ni-Mo alloy films

It is well known that pure metallic Mo cannot be deposited from an aqueous solution because of its high overvoltage than hydrogen. Nevertheless, an alloy can be created by co-depositing Mo with iron-group metals [65]. According to Fekih et al. [66], the amount of Mo increases in Fe-Ni-Mo alloy films as the amount of molybdate in the electrolyte increases. Mo-rich films exhibit strong corrosion resistance, whereas deposit films with low Mo content exhibit good magnetic characteristics. A higher molybdate concentration in the electrolyte promotes the formation of molybdenum oxides, which obstructs the deposition process.

According to Huang et al. [33], the Fe-Ni-Mo alloy films have numerous cracks and microcracks dispersed across the surface. In contrast, the Fe-Ni alloy film exhibits cauliflower-like morphology without cracks, as depicted in Figure 10. The origin of these cracks represents high residual stress in films. The Mo atom would occupy the Ni in the Ni lattice during the electrodeposition process because its radius is more significant than Ni atoms. It would cause the Ni lattice to expand and lead to the creation of cracks. Moreover, the Fe and Mo in the Ni lattice increase the interplanar spacing of the Ni lattice and result in a larger Ni crystal, which broadens the diffraction peaks and shifts the XRD peaks (Figure 11) towards the lower degrees. Peak broadening and shifting suggest that Fe and Mo are the solid solutions in the Ni crystal. According to Badrnezhad et al. [36], a higher Mo content in the deposited film causes more crack propagation during the deposition.

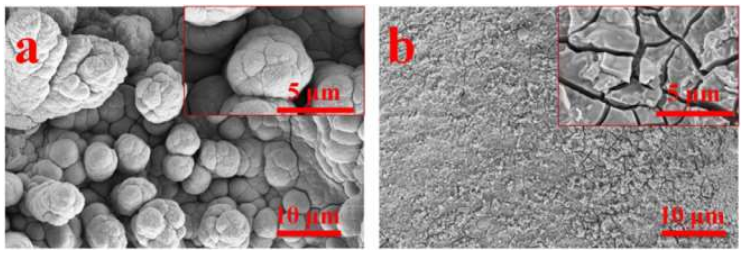

Figure 10 Surface morphology of (a) Fe-Ni film and (b) Fe-Ni-Mo films [33].

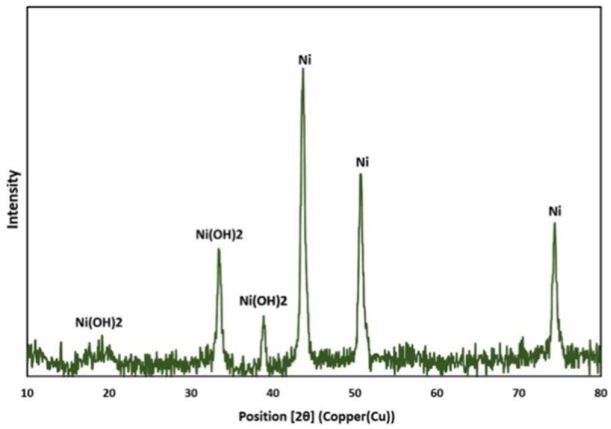

Figure 11 XRD pattern of Fe-Ni-Mo alloy film [36].

The amount of Mo in the deposit impacts the B_S and H_C of the deposited Fe-Ni-Mo alloy films. By raising the Mo concentration in the deposited layer, the B_S drops while the H_C rises [67], [68]. Mo is a non-magnetic alloying element that reduces saturation magnetization. The microstructure changes caused by an increase in the Mo content are responsible for the increase in domain walls pinning, results in an increase in H_C. The content of Mo can be controlled by adjusting the deposition parameters, including current density, pH, deposition time, and concentration of metals in the solution. The Fe and Ni content increases with the Fe-ions and Ni-ions in the electrolyte. The Mo content can be tuned by controlling the concentration of Mo-containing salt [69]. The content of the Fe and Mo increases by raising the current density [36]; however, the Ni content in deposited films decreases [37].

The H_C of Fe-Ni-Mo films also varies by changing the film thickness [54], [70]. The D of the deposited films reduces with the increasing thickness of the films. Zhou et al. [35] reported that the H_C decreases from over 100 Oe for thickness = 32 nm to under 10 Oe for thickness = 107 nm. The H_C is proportional to the effective anisotropy constant, k_{eff}, and this relationship is proposed to cause the decline in coercivity. If D is lower than the exchange length and the grain orientation is random, the k_{eff} decreases.

4. Summary

Fe-Ni-based ternary alloys are promising soft magnetic materials. In these Fe-Ni-based alloys, transition metals such as Co, Cr, Mo, and W are commonly incorporated to improve their properties. Electrodeposition is a widely used technique for the synthesis of these ternary alloys. In the electrodeposition process, the deposition parameters affect the deposited ternary alloys' composition, morphology, and microstructure. The commonly used deposition parameters are current density, additives, concentration of electrolyte, pH, etc. And, the properties of these alloys depend on the morphology, composition, and microstructure of the deposited films.

This chapter discusses soft magnetic Fe-Ni-based ternary alloy films, including Fe-Ni-Co, Fe-Ni-Cr, Fe-Ni-Mo, and Fe-Ni-W deposited by electrodeposition techniques. These alloys' soft magnetic properties strongly depend on the composition, microstructure, and morphology. The

composition of the deposited films depends mainly on the nature of the electrolyte. Chloride and sulfate-based electrolytes are generally utilized to deposit these soft magnetic films. These electrolytes are economical for the deposition of Fe-Ni-based alloy films. The applied current density and composition can tune the microstructure and grain size of the deposited ternary alloy films. The grain size decreases with increasing the current density, which influences the coercivity of the deposited films. And, the saturation magnetization is controlled by the composition of the deposited alloy films.

References:

[1] G. Herzer, Magnetization process in nanocrystalline ferromagnets, *Materials Science and Engineering: A*, 133, 1-5, 1991. DOI: 10.1016/0921-5093(91)90003-6

[2] G. Herzer, Nanocrystalline soft magnetic materials, *Physica Scripta*, T49, 307-314, 1993. DOI: 10.1088/0031-8949/1993/T49A/054

[3] Y. Peng, Z. Zhu, J. Chen, J. Ren, and T. Han, Research on pulse electrodeposition of Fe-Ni alloy, *AIP Advances*, 4, 031301, 2014. DOI: 10.1063/1.4861125

[4] H. X. Wei, L. S. Bin, Y. S. Lin, L. J. Ping, and G. Bo, Electrical and magnetic properties of electrodeposited Fe-based alloys used for thin film transformer, *Science China Technological Sciences*, 56, 84-88, 2013. DOI: 10.1007/s11431-012-5039-7

[5] V. Torabinejad, M. Aliofkhazraei, S. Assareh, M. H. Allahyarzadeh, A. S. Rouhaghdam, Electrodeposition of Ni-Fe alloys, composites, and nano coatings – A review, *Journal of Alloys and Compounds*, 691, 841-859, 2017. DOI: 10.1016/j.jallcom.2016.08.329

[6] C. Su, L. Zhao, L. Tian, B. Wen, M. Xiang, W. Bai, and J. Guo, Rapid electrodeposition of Fe-Ni alloy foils from chloride bath containing trivalent iron ions, *Coatings*, 9 (56), 1-12, 2019. DOI: 10.3390/coatings9010056

[7] E. Yousefi, A. Irannejad, and S. Sharafi, Electrodeposition and characterization of nanocrystalline Fe-Ni-Cr alloy coatings synthesized via pulse current method, *Transactions of Nonferrous Metals Society of China*, 29, 2591-2603, 2019. DOI: 10.1016/S1003-6326(19)65166-6

[8] V. Torabinejad, M. Aliofkhazraei, S. Assareh, M. H. Allahyarzadeh, and A. S. Rouhaghdam, Electrodeposition of Ni-Fe alloys, composites, and nano coatings – A review, *Journal of Alloys and Compounds*, 691, 841-859, 2017. DOI: 10.1016/j.jallcom.2016.08.329

[9] H. Adelkhani and M. R. Arshadi, Properties of Fe-Ni-Cr alloy coatings by using direct and pulse current electrodeposition, *Journal of Alloys and Compounds*, 476, 234-237, 2009. DOI: 10.1016/j.jallcom.2008.09.108

[10] V. Torabinejad, M. Aliofkhazraei, A. S. Rouhaghdam, and M. H. Allahyarzadeh, Tribological properties of Ni-Fe-Co multilayer coatings fabricated by pulse electrodeposition, *Tribology International*, 106, 34-40, 2017. DOI: 10.1016/j.triboint.2016.10.025

[11] S. F. Harty, J. A. Mcgeough, and R. M. Tulloch, A Review of the electroforming of iron and iron-nickel alloy, *Surface Technology*, 12, 39-55, 1981. DOI: 10.1016/0376-4583(81)90135-7

[12] I. Tabakovic, J. Gong, S. Riemer, M. Kautzky, Influence of surface roughness and current efficiency on composition gradients of thin NiFe films obtained by electrodeposition, *Journal of Electrochemical Society*, 162, D102-D108, 2015. DOI: 10.1149/2.0351503jes

[13] T. Nagayama, T. Yamamoto, and T. Nakamura, Thermal expansions and mechanical properties of electrodeposited Fe-Ni alloys in the invar composition range, *Electrochimica Acta*, 205, 178-187, 2016. DOI: 10.1016/j.electacta.2016.04.089

[14] C. Su, F. He, H. Ju, Y. Zhang, E. Wang, Electrodeposition of Ni, Fe and Ni-Fe alloys on a 316 stainless steel surface in a fluorborate bath, *Electrochimica Acta*, 54(26), 6257-6263, 2009. DOI: 10.1016/j.electacta.2009.05.076

[15] C. Su, E. Wang, Y. Zhang, F. He, $Ni_{1-X}Fe_X$ ($0.1<X<0.75$) alloy foils prepared from a fluorborate bath using electrochemical deposition, *Journal of Alloys and Compounds*, 474, 190-194, 2009. DOI: 10.1016/j.jallcom.2008.06.050

[16] M. L. Trudeau, Nanocrystalline Fe and Fe-riched Fe-Ni through electrodeposition, *Nanostructured Materials*, 12, 55-60, 1999. DOI: 10.1016/S0965-9773(99)00065-3

[17] V. M. Dubin, M. O. Lisunova, B. L. Walton, Invar electrodeposition for controlled expansion interconnects, *Journal of Electrochemical Society*, 164, D321-D326, 2017. DOI: 10.1149/2.1271706jes

[18] M. Izaki, Electrodeposition of iron and iron alloys, Modern Electroplating, 5th Edition, M. Schlesinger and M. Paunovic, Wiley, 2010. DOI: 10.1002/9780470602638.ch11

[19] V. Torabinejad, M. Aliofkhazraei, S. Assareh, M. H. Allahyarzadeh, and A. S. Rouhaghdam, Electrodeposition of Ni-Fe alloys, composites, and nano coatings – A review, *Journal of Alloys and Compounds*, 691, 841-859, 2017. DOI: 10.1016/j.jallcom.2016.08.329

[20] R. Abdel-Karim, Y. Reda, M. Muhammed, S. El-Raghy, M. Shoeib, and H. Ahmed, Electrodeposition and Characterization of Nanocrystalline Ni-Fe alloys, *Journal of Nanomaterials*, 519274, 1-8, 2011. DOI: 10.1155/2011/519274

[21] S. D. Leith, S. Ramli, and D. T. Schwartz, Characterization of Ni_xFe_{1-x} ($0.10 < x < 0.95$) Electrodeposition from a Family of Sulfamate-Chloride Electrolytes, *Journal of The Electrochemical Society*, 146, 1431-1435 (1999). DOI: 10.1149/1.1391781

[22] L. Sziraki, E. Kuzmann, M. EI-Sharif, C. U. Chisholm, G. Principi, C. Tosello, A. Vertes, Electrochemical behavior of electrodeposited strongly disordered Fe–Ni–Cr alloys, *Electrochemistry Communications*, 2, 619-625 (2000). DOI: 10.1016/S1388-2481(00)00088-6

[23] E. Bertero, M. Hasegawa, S. Staubli, E. Pellicer, I. K. Herrmann, J. Sort, J. Michler, L. Philippe, Electrodeposition of amorphous Fe-Cr-Ni stainless steel alloy with high corrosion resistance, low cytotoxicity and soft magnetic properties, *Surface & Coatings Technology*, 349, 745-751 (2018). DOI: 10.1016/j.surfcoat.2018.06.003

[24] C. A. Huang, J. H. Chang, C. Y. Chen, K. Y. Liao, J. Mayer, Microstructure and electrochemical corrosion behavior of Cr–Ni–Fe alloy deposits electroplated in the presence of trivalent Cr ions, *Thin Solid Films*, 544, 69-73 (2013). DOI: 10.1016/j.tsf.2013.04.124

[25] M. Tavoosi and A. Barahimi, Corrosion behavior of amorphous–nanocrystalline Fe–Ni–Cr electrodeposited coatings, *Surfaces and Interfaces*, 8, 103-111 (2017). DOI: 10.1016/j.surfin.2017.05.004

[26] E. V. Khomenko, E. E. Shalyguina, and N. G. Chechenin, Magnetic properties of thin Co-Fe-Ni films, *Journal of Magnetism and Magnetic Materials*, 316, 451-453, 2007. DOI: 10.1016/j.jmmm.2007.03.117

[27] D. -Y. Park, B. Y. Yoo, S. Kelcher, and N. V. Myung, Electrodeposition of low-stress high magnetic moment Fe-rich FeCoNi thin films, *Electrochimica Acta*, 51, 2523-2530, 2006. DOI: 10.1016/j.electacta.2005.07.037

[28] X. Sun, Z. Li, F. Xu, and Y. Wang, Spin and orbital moments of electrodeposited Fe28Co51Ni21 soft magnetic films determined by X-ray magnetic circular dichroism, *Journal of Alloys and Compounds*, 656, 812-817 (2016). DOI: 10.1016/j.jallcom.2015.09.196

[29] K. R. Sriraman, S. G. S. Raman, and S. K. Seshadri, Corrosion behavior of electrodeposited nanocrystalline Ni-W and Ni-Fe-W alloys, *Materials Science and Engineering A*, 460-461, 39-45, 2007. DOI: 10.1016/j.msea.2007.02.055

[30] F. He, J. Yang, T. Lei, and C. Gu, Structure and properties of electrodeposited Fe-Ni-W alloys with different levels of tungsten content: a comparative study, *Applied Surface Science*, 253, 7591-7598, 2007. DOI: 10.1016/j.apsusc.2007.03.068

[31] B. M. Mundotiya, L. Rissing, and M. C. Wurz, Effect of substrate temperature on magnetic properties of electroplated 82Ni-15Fe-3W alloy films, *IEEE Transactions on Magnetics*, 52, 2003305, 2016. DOI: 10.1109/TMAG.2016.2549987

[32] L. R. Zelenovic, N. Cirovic, M. Spasojevic, N. Mitrovic, A. Maricic, and V. Pavlovic, Microstructural properties of electrochemically prepared NieFeeW powders, *Materials Chemistry and Physics*, 135, 212-219 (2012). DOI: 10.1016/j.matchemphys.2012.04.061

[33] Y. Huang, Y. Wu, Z. Zhang, L. Yang, Q. Zang, Rapid electrodeposited of self-supporting Ni-Fe-Mo film on Ni foam as affordable electrocatalysts for oxygen evolution reaction, *Electrochimica Acta*, 390, 138754 (2021). DOI: 10.1016/j.electacta.2021.138754

[34] R. Kannan, M. Selvambikai, E. Selva Kumar, S. Venkateshwaran, Synthesis, structural and mechanical properties of electroplated NiFeMo nanocrystalline thin films, *International Journal of Innovative Technology and Exploring Engineering*, 8, 100-103 (2019). DOI: 10.35940/ijitee.K1022.09811S19

[35] Q. Zhou, J. Velleuer, P. J. Heard, and W. Schwarzacher, Surface Roughness and Magnetic Properties of Electrodeposited NiFeMo Thin Films, *Electrochemical and Solid-State Letters*, 12, D7-D10 (2009). DOI: 10.1149/1.3050351

[36] R. Badrnezhad, F. Nasri, H. Pourfarzad, S. K. Jafari, Effect of iron on Ni–Mo–Fe composite as a low-cost bifunctional electrocatalyst for overall water splitting, *International Journal of Hydrogen Energy*, 46, 3821-3832 (2021). DOI: 10.1016/j.ijhydene.2020.10.174

[37] W. Hu, Y. Zhang, D. Song, Z. Zhou, Y. Wang, Electrode properties of amorphous Ni-Fe-Mo alloy as hydrogen electrocatalyst in alkaline solution, *Materials Chemistry and Physics*, 41, 141-145 (1995). DOI: 10.1016/0254-0584(95)80019-0

[38] I. Vernyhora, V. Tatarenko, S. Bokoch, Thermodynamics of fcc-NieFe alloys in a static applied magnetic field, *ISRN Thermodynamics*, 2012, 0-11 (2012). DOI: 10.5402/2012/917836.

[39] V. Torabinejad, M. Aliofkhazraei, S. Assareh, M. H. Allahyarzadeh, and A. S. Rouhaghdam, Electrodeposition of Ni-Fe alloys, composites, and nano coatings - A review, *Journal of Alloys and Compounds*, 691, 841-859 (2017). DOI: 10.1016/j.jallcom.2016.08.329

[40] A. Chenna, N. Benbrahim, l. Hamadou, S. Boudinar, A. Kadri, E. Chainet, and Y. Dahmane, Characterisation of electroplated Ni45Fe55 thin films on n-Si (111), *Surface Engineering*, 35, 189-198, 2019. DOI: 10.1080/02670844.2018.1442306

[41] B. Koo, B. Yoo, Electrodeposition of low-stress NiFe thin films from a highly acidic electrolyte, *Surface and Coating Technology*, 205, 740-744, 2010. DOI: 10.1016/j.surfcoat.2010.07.076

[42] X. Su and C. Qiang, Influence of pH and bath composition on properties of Ni-Fe alloy films synthesized by electrodeposition, *Bulletin of Materials Science*, 35, 183-189, 2012. DOI: 10.1007/s12034-012-0284-8

[43] T. Shimokawa, T. Yanai, K. Takahashi, M. Nakano, K. Suzuki, and H. Fukunaga, Soft magnetic properties of electrodeposited Fe-Ni films prepared in citric acid based bath, *IEEE Transactions on Magnetics*, 48, 2907-2909 (2012). DOI: 10.1109/TMAG.2012.2203295

[44] Y. Sknar, I. Sknar, A. Cheremysinova, I. Yermolenko, and A. Sachanova, Research into composition and properties of the Ni-Fe electrolytic alloy, *Eastern-European Journal of Enterprise Technologies*, 88, 4-12, 2017. DOI: 10.15587/1729-4061.2017.106864

[45] T. E. Buchheit, S. H. Goods, P. G. Kotula, and P. F. Hlava, Electrodeposited 80Ni–20Fe (Permalloy) as a structural material for high aspect ratio microfabrication, *Materials Science and Engineering A*, 432, 149-157 (2006). DOI: 10.1016/j.msea.2006.05.149

[46] G. Saravanan and S. Mohan, Electrodeposition of Fe-Ni-Cr alloy from deep eutectic system containing choline chloride and ethylene glycol, *International Journal of Electrochemical Science*, 6, 1468-1478, 2011.

[47] C. A. Snavely, A theory for the mechanism of chromium plating - a theory for the physical characteristics of chromium plate, *Transactions of The Electrochemical Society*, 92, 537-577 (1947). DOI: 10.1149/1.3071841

[48] D. Shu-hao and G. Zhu-qing, The electrochemical behavior of pulse-plated nanocrystalline iron-nickel-chromium alloy, *Anti-Corrosion Methods and Materials*, 50, 267-270, 2003. DOI: 10.1108/00035590310482497

[49] S. Atalay, H. Gencer, V. S. Kolat, Magnetic entropy change in $_{Fe74-x}Cr_xCu_1Nb_3Si_{13}B_9$ (x = 14 and 17) amorphous alloys, *Journal of Non-Crystalline Solids*, 351, 2373-2377 (2005). DOI: 10.1016/j.jnoncrysol.2005.07.012

[50] Y. Boliang, J. M. D. Coey, M. Olivier, J. O. Ström-Olsen, Onset of magnetism in iron-chromium glasses, *Journal of Applied Physics*, 55, 1748-1750 (1984). DOI: 10.1063/1.333464

[51] E. Yousefi, S. Sharafi, A. Irannejad, Microstructure, tribological behavior and magnetic properties of Fe−Ni−TiO2 composite coatings synthesized via pulse frequency variation, *Transactions of Nonferrous Metals Society of China*, 31, 3800-3813 (2021). DOI: 10.1016/S1003-6326(21)65765-5

[52] R. Mardani, A. Asrar, and H. Ershadifer, The effect of surfactant on the structure, composition and magnetic properties of electrodeposited CoNiFe/Cu microwire, *Materials Chemistry and Physics*, 211, 160-167, 2018. DOI: 10.1016/j.matchemphys.2018.02.026

[53] Y. Zhang and D. G. Ivey, Characterization of Co-Fe and Co-Fe-Ni soft magnetic films electrodeposited from citrate-stabilized sulfate baths, *Materials Science and Engineering B*, 140, 15-22, 2007. DOI: 10.1016/j.mseb.2007.03.004

[54] I. Tabakovic, V. Inturi, S. Riemer, Composition, structure, stress, and coercivity of electrodeposited soft magnetic CoNiFe films thickness and substrate dependence, *Journal of Electrochemical Society*, 149, C18-C22, 2002.

[55] J. Gong, S. Riemer, A. Morrone, V. Venkatasamy, M. Kautzky, I. Tabakovic, Composition gradients and magnetic properties of 5-100nm thin CoNiFe films obtained by electrodeposition, *Journal of Electrochemical Society*, 159, D447-D454, 2012.

[56] K. Ohashi, Y. Yasue, M. Saito, K. Yamada, T. Osaka, M. Takai, K. Hayashi, Newly developed inductive write head with electroplated CoNiFe film, *IEEE Transactions on Magnetics*, 34, 1462-1464 (1998). DOI: 10.1109/20.706583

[57] X. Liu, G. Zangari, L. Shen, Electrodeposition of soft, high moment Co–Fe–Ni thin films, *Journal of Applied Physics*, 87, 5410 (2000). DOI: 10.1063/1.373359

[58] R. M. Bozorth, Ferromagnetism, Vol. V, D. Van Nostrand Company, New York, 1951, p. 160.

[59] T. Osaka, Electrodeposition of highly functional thin films for magnetic recording devices of the next century, *Electrochimica Acta*, 45, 3311-3321, 2000. DOI: 10.1016/S0013-4686(00)00407-2

[60] H. Kockar, O. Demirbas, H. Kuru, M. Alper, O. Karaagac, M. Haciismailoglu, and E. Ozergin, Electrodeposited NiCoFe films from electrolytes with different Fe ion concentrations, *Journal of Magnetism and Magnetic Materials*, 360, 148-151, 2014. DOI: 10.1016/j.jmmm.2014.01.078

[61] M. Saito, K. Yamada, K. Ohashi, Y. Yasue, Y. Sogawa, and T. Osaka, Corrosion properties of electroplated CoNiFe films, *Journal of the Electrochemical Society*, 146, 2845-2848, 1999. DOI: 10.1149/1.1392018

[62] F. E. Rasmussen, J. T. Ravnkilde, P. T. Tang, O. Hansen, S. Bouwstra, Electroplating and characterization of cobalt–nickel–iron and nickel–iron for magnetic microsystems applications, *Sensors and Actuators A: Physical*, 92, 242-248 (2001). DOI: 10.1016/S0924-4247(01)00556-8

[63] M. Donten, H. Cesiulis, and Z. Stojek, Electrodeposition and properties of Ni-W, Fe-W and Fe-Ni-W amorphous alloys: a comparative study, *Electrocjimica Acta*, 45, 3389-3396, 2000. DOI: 10.1016/S0013-4686(00)00437-0

[64] P. Esther, C. J. Kennady, P. Saravanan, and T. Venkatachalam, Structural and magnetic properties of electrodeposited Ni-Fe-W thin films, *Journal of Non-Oxide Glasses*, 1, 301-309 (2009).

[65] M. H. Allahyarzadeh, B. Roozbehani, A. Ashrafi, S. R. Shadizadeh, Electrodeposition of high Mo content amorphous/nanocrystalline Ni–Mo alloys using 1- methyl - imidazolium chloride ionic liquid as an additive, *Surface and Coatings Technology*, 206, 137-142 (2011). DOI:10.1016/j.surfcoat.2011.07.004

[66] Z. Fekih, N. Ghellai, S. Sam, N. E. Chabanne, N. Gabouze, The iron-nickel molybdenum (Fe-Ni-Mo) electrodeposited alloy on n-type silicon, *Advances In Materials Science*, 12, 17-26 (2012). DOI: 10.2478/v10077-012-0002-7

[67] R. Mardani, H. Shahmirzaee, H. Ershadifer, M. R. Vahdani, Electrodeposition of Ni32Fe48Mo20 and Ni52Fe33W15 alloy film on Cu microwire from ionic liquid containing plating bath, *Surface and Coatings Technology*, 324, 281-287 (2017). DOI: 10.1016/j.surfcoat.2017.05.087

[68] I. Bursuc, G. Caluaru, C. Cuciureanu, Magnetization of Ni-Fe-Mo electrolytic films at low temperatures, *IEEE Transactions on Magnetics*, 7, 309-310 (1971). DOI: 10.1109/TMAG.1971.1067045

[69] H. L. Seet, X. P. Li, H. J. Neo, and K. S. Lee, Magnetic properties of high permeability NiFeMo/Cu composite wires, *Journal of Alloys and Compounds*, 449, 96-100 (2008). DOI: 10.1016/j.jallcom.2006.01.126

[70] Q. Zhou, P. J. Heard, and W. Schwarzacher, Fabrication and magnetic properties of patterned NiFeMo films electrodeposited in self-assembled nanosphere templates, *Journal of Applied Physics*, 109, 054313 (2011). DOHuaI: 10.1063/1.3561362